RESEARCH COMMUNICATIONS

Carbon dioxide observations at Cape Rama, India for the period 1993–2002: implications for constraining Indian emissions

Yogesh K. Tiwari[1],*, **Prabir K. Patra[2],**
Frédéric Chevallier[3], Roger J. Francey[4],
Paul B. Krummel[4], Colin E. Allison[4],
J. V. Revadekar[1], Supriyo Chakraborty[1],
Ray L. Langenfelds[4], S. K. Bhattacharya[5],
D. V. Borole[6], K. Ravi Kumar[1] and L. Paul Steele[4]

[1]Centre for Climate Change Research,
Indian Institute of Tropical Meteorology, Pune 411 008, India
[2]Research Institute for Global Change, JAMSTEC, Yokohama, Japan
[3]Laboratoire des Sciences du Climat et de l'Environnement,
CEA-CNRS-UVSQ, IPSL, Gif-sur-Yvette, France
[4]Centre for Australian Weather and Climate Research,
CSIRO Marine and Atmospheric Research, Aspendale, Australia
[5]Physical Research Laboratory, Ahmedabad 380 009, India
[6]National Institute of Oceanography, Goa 403 004, India

India has the second largest population, one of fastest growing economies and is ranked third in greenhouse gas emissions by fossil-fuel burning in the world. However, there has been little monitoring of atmospheric CO_2 concentration over India to date. Here we reanalyse pioneering atmospheric CO_2 observations at Cape Rama, India (CRI) during the period from February 1993 to October 2002, using three forward transport models to simulate atmospheric CO_2 and separate tracers of terrestrial and oceanic fluxes, and fossil-fuel emissions. The CO_2 seasonal behaviour at this site has clear signals from monsoon-driven meteorology and terrestrial ecosystem activity, which are generally captured by all three models. The quality of the agreement between the simulations and the observations varies with season, with better results obtained during the southwest monsoon months when the CRI site observes the oceanic air of mostly southern hemispheric origin. Relatively poor model-data agreements in the other seasons, when air originating from the Indian subcontinent passes over the site, arise from the inability of coarse-resolution global models to represent CRI appropriately. In addition, limited atmospheric CO_2 measurements in the South Asia region only provide poor constraint on inversion fluxes. Flux signal footprint analysis of the CRI station highlights the need of extending the observation network inland and to different parts of the country for better understanding of the carbon cycle of India.

Keywords: Asian carbon cycle, CO_2 observation, forward transport model.

INDIA is the largest growing economies in South Asia, supporting a population of around 1.2 billion and experiencing a steep rise in energy demand. The Carbon Dioxide Information Analysis Center (CDIAC), USA, estimates the total fossil-fuel CO_2 emissions from India as 189 TgC in 1990, 324 TgC in 2000, 385 TgC in 2005 and 508 TgC in 2009, and the annual rate of increase as ~7% per year during 2005–2009 (ref. 1). Some of these emissions may be compensated by vegetation uptake[2,3]. Quantifying the carbon balance between the emissions of industry and transport, and the ecosystem uptake in India is an important step towards the design of effective greenhouse gas mitigation strategies in this subcontinent.

Contributing to this goal, the Australian Commonwealth Scientific and Industrial Research Organisation (CSIRO) in collaboration with the Physical Research Laboratory (PRL), Ahmedabad and National Institute of Oceanography (NIO), Goa, established an air-sampling station at Cape Rama, India, (CRI; 73.9°E, 15.1°N) in 1993, to monitor the concentrations of CO_2 and other trace-gas species. The station operated for 10 years, i.e. till 2002 (ref. 4). Air sampling at CRI contributed to the Global Atmosphere Watch (GAW) programme of the World Meteorological Organization that monitors the global atmospheric composition, and the measurements have been archived in World Data Centre for Greenhouse Gases, Japan (WDCGG; http://gaw.kishou.go.jp/wdcgg/).

CRI is a coastal site located at the eastern boundary of the Arabian Sea, on the west coast of India, off Goa. Arabian Sea winds have a particularly strong seasonality, the amplitude of which is rarely found elsewhere[5]. Terrain-induced phenomena, such as sea–land breezes makes the representation of coastal sites in atmospheric models quite difficult, and interpretation of the data is compromised by the lack of regional terrestrial models and of validated high-resolution transport modelling around the CRI site. However, the historic nature of these data, from a rapidly evolving region of the globe, justifies their examination within the framework of current global carbon models, both as a way of estimating the past regional budget, and for identifying modelling and measurement methods that will enhance information on regional and global carbon budgets in the future. In this study, we have compared CRI CO_2 observations for the period 1993–2002 with three different forward model simulations to explore the challenges facing observational and modelling efforts in order to link Indian emissions to the large-scale atmospheric behaviour.

The observing site, CRI is located near the seashore on the west coast of India (Figure 1, marked with black circle) and about 60 m amsl. The site is free from any major vegetation and is away from habitation. Details are available in Bhattacharya et al.[6], and only a brief summary is provided here. Sampling is conducted all year round when winds are onshore. There is a seasonal reversal in large-scale wind patterns: from June to September, during the southwest (SW) monsoon, the sampling site receives air masses having predominantly marine
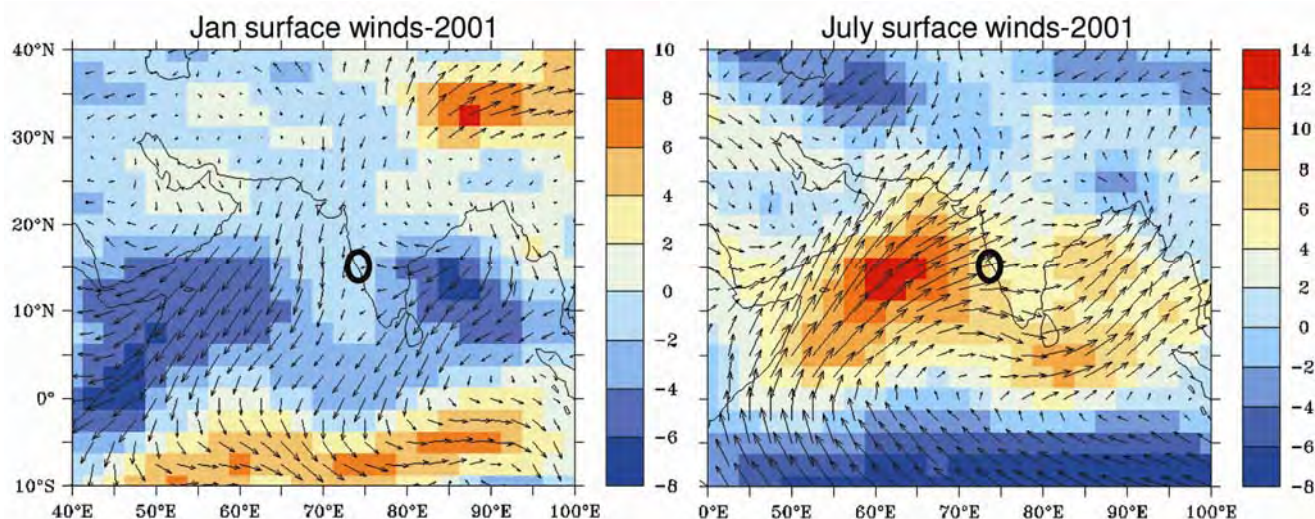
Figure 1. NOAA NCEP-derived monthly mean *u*-wind at the surface during winter (left panel) and monsoon month (right panel). Arrows indicate wind direction. Station CRI (Cape Rama, India) is marked with a black circle.

signatures (Figure 1, right panel), while from November to February, during the northeast (NE) monsoon (i.e. winter), a westerly sea breeze is sampled comprising recycled air mainly from the Indian subcontinent (Figure 1, left panel). The mean wind speed at the time of sampling at the surface is about 10–12 m s^{-1} during the SW monsoon and about 4–6 m s^{-1} during the rest of the year[6].

When the site was active, air samples were collected in two separate 0.5 litre glass flasks, 6 m above ground twice per month. The filled glass flasks were analysed at the then CSIRO Atmospheric Research GASLAB (Global Atmospheric Sampling LABoratory) in Australia for measurement of the concentration of CO_2 and other trace gases[4].

In July 2009, CRI observations were revived by CSIRO and NIO, and the recent data will be submitted to GAW after sufficient quality control. Up-to-date data might be obtained for specific studies by contacting CSIRO scientists (P.B.K. or L.P.S.).

Regular sampling at CRI started in February 1993, and pair of air samples were collected bi-monthly until October 2002. The CO_2 concentration data from 1993 to 2002 are presented here as is and in the form of a spline fit to individual flask data, and compared with simulated atmospheric CO_2 (Figure 2). The spline fit consists of two components, increasing trend and seasonal cycle. Both components were obtained by least-squares fitting of a linear function combined with harmonics as below:

$$CO_2(t) = \underbrace{a_0 + a_1 t + a_2 t^2}_{\text{trend}} + \underbrace{\sum_{n=1}^{4} [b_n \cdot \sin(2\pi n\omega t) + c_n \cdot \cos(2\pi n\omega t)]}_{\text{seasonal cycle}}. \quad (1)$$

The fitting method accounts for harmonics associated with seasonal forcing of the CO_2 levels separately from trends, consisting of the long-term increase associated with anthropogenic emissions and from interannual variation that has been associated with ENSO (droughts, wild fires, etc.) and volcanic activity[7].

The atmospheric CO_2 concentrations are modelled for this study using three different transport models with different surface fluxes. To perform a proper comparison between CRI observations and model simulations, the simulations are sampled at co-located latitude, longitude, and time of air sampling. The main differences among the models are: (1) the spatial resolution, with TM3 having coarser resolution than LMDZ and ACTM models; (2) the LMDZ and ACTM models are a full GCM, whereas TM3 is an offline model, and (3) the meteorological fields used to drive the model transport differ. The specifications for each simulation are described next. For simplicity, each simulation will be called by the name of the corresponding transport model in the following, even though the CO_2 surface fluxes are also specific.

Simulation TM3: In the TM3 transport model of the Max Planck Institute, Germany[8], atmospheric CO_2 concentration is simulated corresponding to the CO_2 fluxes estimated using a time-dependent Bayesian inversion technique[9]. The horizontal resolution of TM3 is $4° \times 5°$ latitude by longitude with 19 sigma-coordinate layers in the vertical. Transport in TM3 is driven by meteorological fields from National Center for Environmental Predictions (NCEP) reanalysis[10]. Using essentially the same method as described in Rödenbeck *et al.*[9], the CO_2 surface fluxes of the atmospheric transport inversion model[11] vary monthly, and cover the period from 1991 to 2003. The fluxes are based on near-surface CO_2 concentration data from 39 selected stations of the NOAA/ESRL (Earth
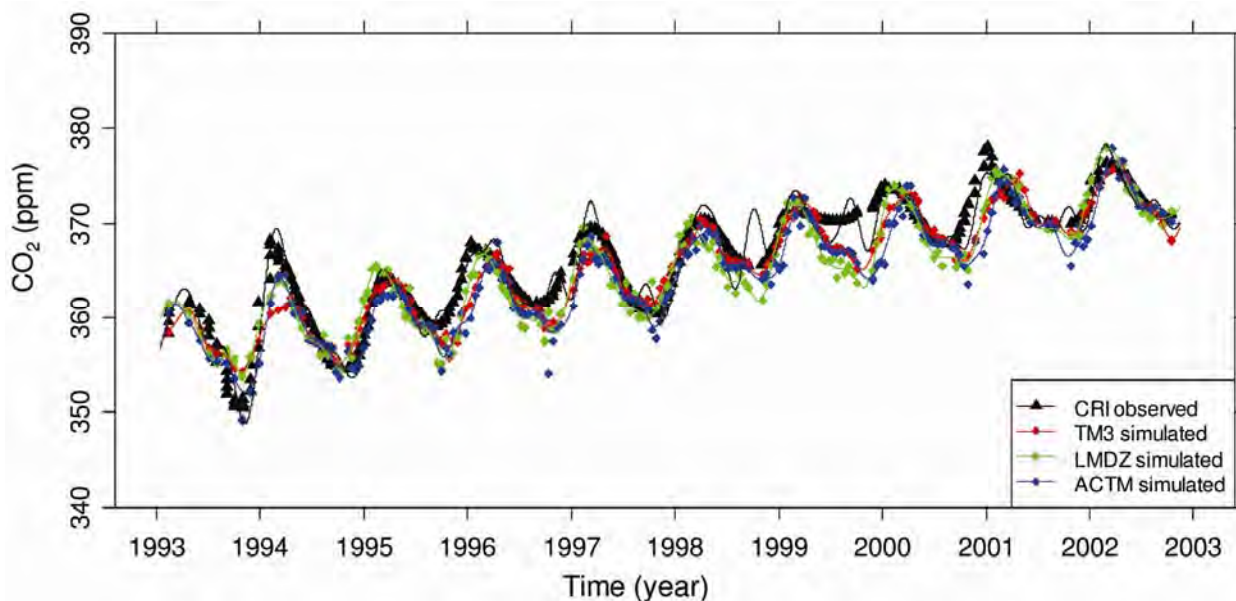
Figure 2. Measured and simulated CO_2 concentration data from 1993 to 2002 (symbols) and spline fit (solid lines) to individual flask data.

System Research Laboratory) network[12] and use the TM3 model transport.

Simulation LMDZ: The general circulation model of the Laboratoire de Météorologie Dynamique (LMDZ)[13] has horizontal resolution of 2.5° × 3.75° (latitude by longitude) and 19 hybrid coordinate layers in the vertical. This model solves the full dynamic equations for all meteorological parameters (e.g. winds, temperature, clouds). The model-calculated winds are nudged towards the winds analysed by the European Centre for Medium-range Weather Forecasts (ECMWF) with a relaxation time of 2.5 h, in order to represent the transport as realistically as possible[14]. The fluxes used for the simulation are estimated using a variational data assimilation technique for the period 1988–2007 (ref. 15). The grid-point flux estimation method uses surface measurements of mixing ratios in individual samples of air collected about every week at various places in the world over land and over ocean as a part of NOAA/ESRL cooperative air sampling network. Measurements are used in the inversion system as they are provided by the NOAA/ESRL without any correction or filter. The uncertainty assigned to each observation within the inversion system includes an estimated measurement error, the error of the transport model that simulates it and the representativeness error, i.e. the mismatch between the scale of the measure and the scale of the transport model.

Simulation ACTM: The Center for Climate System Research/National Institute for Environmental Studies/ Frontier Research Center for Global Change (CCSR/ NIES/FRCGC) Atmospheric General Circulation Model (AGCM)[16]-based Chemistry Transport Model (ACTM)[17] simulates CO_2 and other greenhouse gases in the altitude range of the earth's surface to the mesosphere (~ 90 km). The horizontal resolution of ACTM is 2.8° × 2.8° latitude by longitude with 67 pressure-sigma layers in the vertical. The surface fluxes used for this simulation are estimated following the 22-region cyclostationary time-dependent inverse model[18], but using atmospheric CO_2 data from a network of 87 stations for the period 1999–2001 (ref. 19).

Regular sampling at CRI started in February 1993. Pairs of air samples were collected until October 2002, twice every month. The CO_2 concentration data are presented here in comparison with simulated atmospheric CO_2 along with the fits to each of the time series (Figure 2). On account of seasonal cycle, CO_2 concentration starts increasing in November and peaks in April, whereas it starts decreasing from May onwards and reaches a minimum in October. Monotonous increasing trend is seen from 1993 to 2002. The trend and seasonal cycle show similar patterns for observations and model results. It also exhibits a strong seasonal variation with peak-to-peak amplitude of about 9 ppm. However, simulated time series varies smoothly in time, while the observations show large month-to-month fluctuations with non-systematic extra scatter in some years. The CRI seasonality appears particularly large in 1994/95 (20 ppm) and 1997/98 (13 ppm), which is not reflected in the simulations, but these periods were marked by unusual global wildfire activity[20], particularly at low latitudes. The mean seasonal cycles for observed and model CO_2 over CRI for the period 1993–2002 are shown in Figure 3 a. Mean is taken after removing the trends estimated by spline fitting from the time series. The mean seasonal cycle has a March maximum for the observations and ACTM
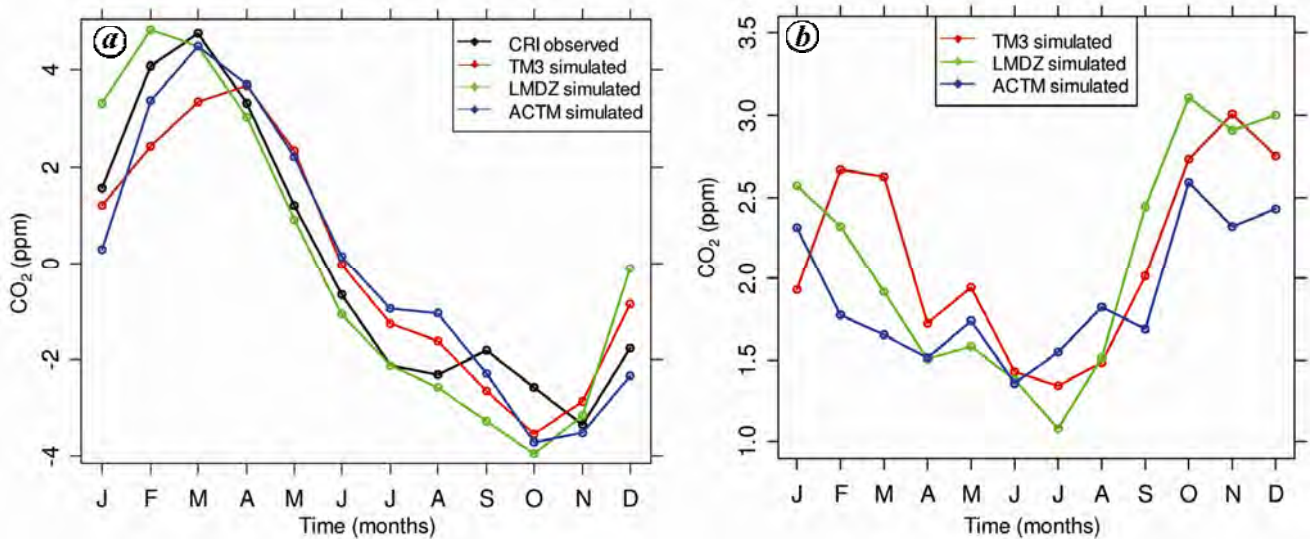
Figure 3. *a*, De-trended mean seasonal cycle of CO_2 (ppm) at CRI during February1993–October 2002, measured through air samples and simulated by TM3, LMDZ and ACTM simulations. *b*, Root mean square difference between modelled and measured CO_2 (ppm) mixing ratio at CRI.

simulations, while the maximum occurs in February for LMDZ simulations, and in April for TM3 simulations. The simulations and observations have a minimum in October and November respectively (Figure 3 *a*). In order to quantify the differences between observed and simulated values (shown here in Figure 3 *a*), we computed the root mean square (RMS) of the differences, for each month (Figure 3 *b*). During the Indian summer monsoon months (June–September), the agreement between model and observed seasonal cycle is better (RMS values within ~1.5 ppm) compared to that for the winter months (RMS values of 2–3 ppm). Simulations agree well with each other (RMS values within 1 ppm) compared to their difference with observations. Generally, all the models capture the CO_2 seasonal cycle at CRI; the square of the correlation coefficient (R^2) between simulated and observed time series ranges between 0.58 and 0.68 for different transport models, and that between the models is always higher ($R^2 \sim 0.84$–0.86).

Three separate tracers for land ecosystem flux, oceanic exchange and fossil-fuel emissions are simulated using ACTM and surface CO_2 fluxes. Comparison between them is made in Figure 4 *a* by presenting the mean seasonal cycle for each of them. This has been used to identify the flux which provides maximum contribution towards the seasonal cycle of CO_2 at the observation site, and to suggest which fluxes may provide minor contributions. Figure 4 *a* shows that the oceanic tracer is not expected to have a measurable impact on the CRI seasonal cycle because the oceanic flux seasonality is weaker in the eastern Arabian Sea compared to its western side off the Oman coast[21]. Additionally, as the oceanic flux map ($4° \times 5°$) and the transport model resolution are coarse, fine scale coastal upwelling is not well represented in this

region. This indicates that the main seasonal forcing at CRI comes from the terrestrial biosphere. This is also corroborated from the strong anti-correlation of the seasonal cycles of $\delta^{13}C$ and CO_2 (Figure 4 *b*). Such strong anti-correlation results mainly from (terrestrial) biospheric activities[6]. Figure 4 *c* shows carbon monoxide (CO) climatological mean observed at CRI during 1993–2002. During the SW monsoon months CO shows minimum values at CRI, whereas during winter months it shows maxima. CO sources are closely linked to those of fossil-fuel CO_2, but CO has stronger sink during summer months compared to the winter due to greater chemical loss by the reaction with OH. As expected from the wind climatology (Figure 1), the seasonal fossil emission signal is expected to be captured during autumn through spring seasons, but not during the summer when the strong trade winds flow from the SW direction, as revealed by Figure 4 *a* (golden line).

The effect of a land tracer signal at the CRI site is not so straightforward. Because the terrestrial ecosystem productivity is water-stressed and almost entirely monsoon-driven in most parts of India, a strong sink in CO_2 is expected during the SW monsoon through the autumn months by forests and intense agricultural activities[3]. However, the CRI site does not capture most of the summer season uptake when the monsoonal SW wind has long ocean trajectories. Thus the strongest influence of terrestrial CO_2 uptake signal appears during October–December at CRI. The ecosystem becomes water-stressed from January until the appearance of the SW monsoon in June, resulting in a net terrestrial carbon release, and thus the contribution to the CO_2 seasonal cycle is similar to that of the fossil tracer. This analysis confirms that during SW monsoon months, the site by itself would not provide

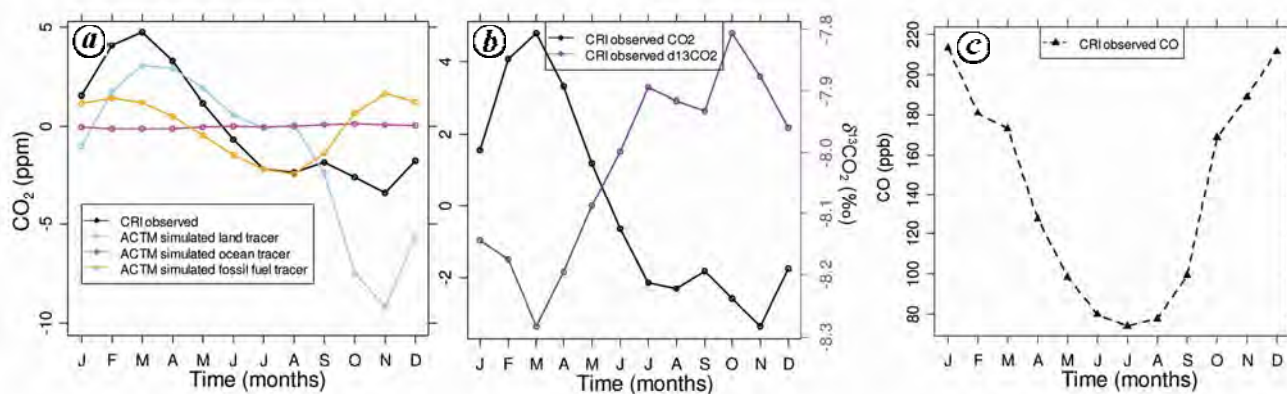**Figure 4.** *a*, ACTM simulated separate land, ocean and fossil-fuel CO_2 components compared with CO_2 (ppm) observations at CRI. *b*, CRI-observed $\delta^{13}CO_2$ (‰) compared with CRI-observed CO_2 (ppm). *c*, CRI-observed CO (ppb).
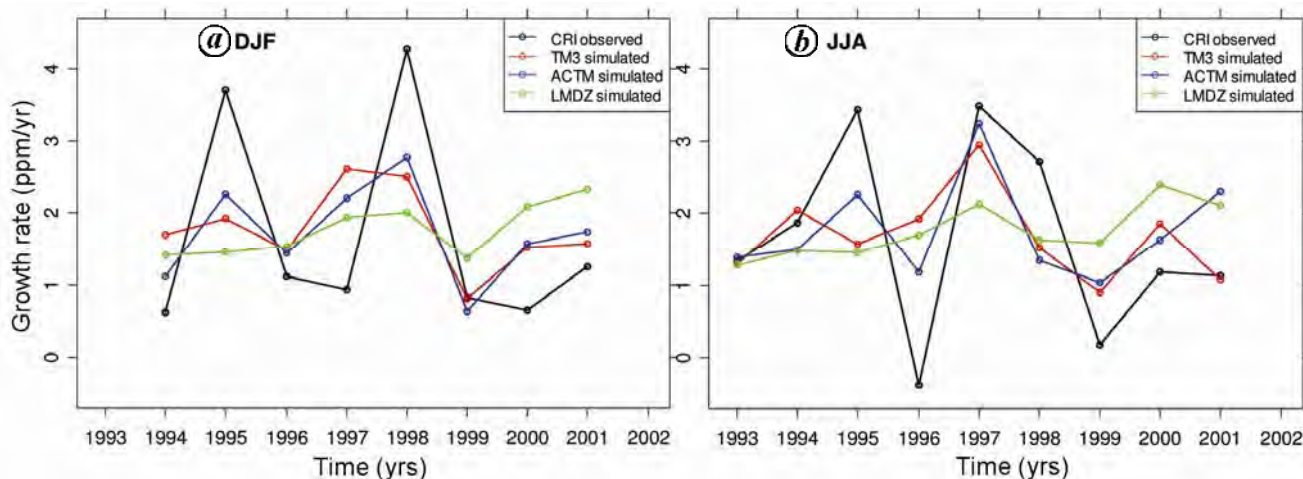

Figure 5. Comparison of mean growth rate of atmospheric CO_2 observed and simulated at CRI during 1993–2002 for (*a*) winter months December–January–February (DJF) and (*b*) summer months June–July–August (JJA).

a significant constraint on flux estimation for the Indian region[22].

Figure 5 shows a comparison of atmospheric CO_2 growth rate during 1993–2002, averaged over December–January–February (DJF), i.e. winter months (Figure 5 *a*) and June–July–August (JJA), i.e. summer months (Figure 5 *b*). Two contrasting seasons for this analysis are chosen for understanding the role of dominant flux components (biosphere during the JJA and fossil-fuel emission during DJF, as seen from Figure 4) on CO_2 growth rates at CRI. Growth rates are calculated by taking the time-derivative of the seasonally averaged values over adjacent DJF and JJA months for each year. The 1994 DJF growth rate represents average of Dec-1993, Jan-1994 and Feb-1994, whereas 1997 growth rate represents average of Dec-1996, Jan-1997 and Feb-1997; similarly for the other years. Variations observed in the atmospheric CO_2 growth rate are primarily controlled by changes in the flux of CO_2 between the atmosphere and terrestrial biosphere and/or

interannual variations in transport. El Niño Southern Oscillation (ENSO) events are a major source of interannual variability in atmospheric CO_2 growth rate due to their effects on terrestrial fluxes through land and ecosystem temperatures, precipitation and incidence of fires. Generally, the mature stage of El Niño events leads to maxima of atmospheric CO_2 growth rates and minima by La Niña events. CO_2 growth rates observed during winter months are higher during 1995 and 1998 and lower during 1997 and 2000. Whereas CO_2 growth rates observed during summer months are higher during 1995 and 1997 and lower during 1996 and 1999. TM3 and ACTM do better than LMDZ with amplitude (Figure 5), may be because it captures the seasonality over the Northern Hemisphere better than LMDZ. Simulations show weak maxima and minima and differ with observations for various years. Noting that ACTM simulation did not include interannual variability in terrestrial biosphere and oceanic fluxes (emissions due to fossil-fuel burning have weak
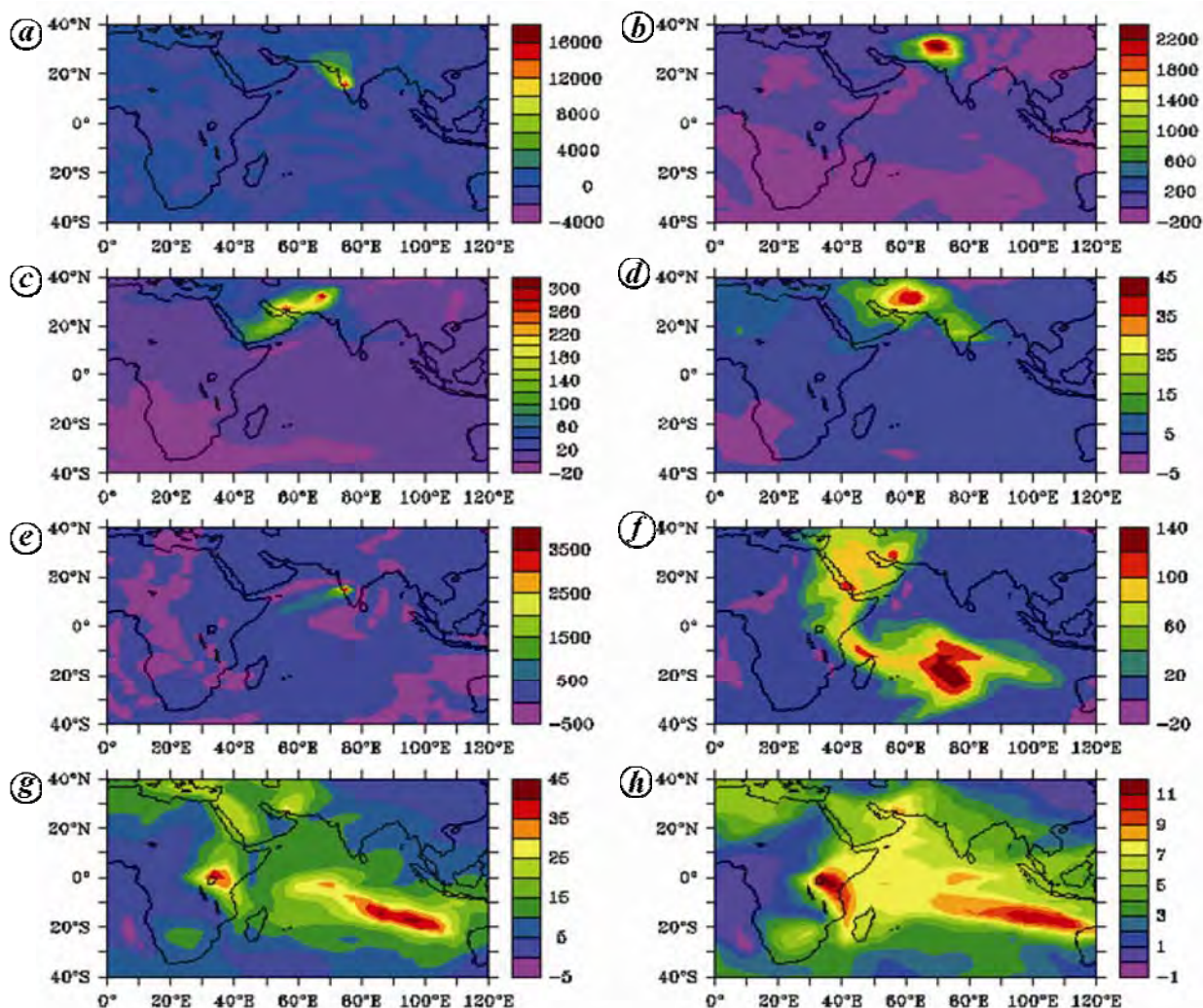
Figure 6. Climatology of Jacobians computed by the adjoint of the LMDZ model for January (*a–d*) and June (*e–h*). Each sequence (*a–d*) and (*e–h*) shows the map of the partial derivatives, in ppm/(kg/m^2/h), of a 24-h mean concentration at CRI with respect to CO$_2$ surface fluxes in the previous week (*a, e*), two weeks before (*b, f*), three weeks before (*c, g*) and four weeks before (*d, h*).

variability in the model), and exhibiting the best correlation coefficients for both seasons suggest the transport variabilities play significant role in interannual variations in CO$_2$ concentrations at CRI.

Figure 6 shows maps of transport derivatives (i.e. maps of the derivatives of the concentration with respect to the surface fluxes at a particular date) using the LMDZ transport model at CRI. They have been computed in the following way. For January and June 2008, a synthetic continuous observation on the 28th was generated for 24 h and used as an input to the adjoint model of LMDZ. The adjoint model was run backward in time from each date. The resulting maps of transport sensitivities are shown as averages per 8-day periods. Week 0 corresponds to the period centred on 25th. Week 1 corresponds to the period centred on the 17th. Week 2 corresponds to the period centred on the 9th. Week 3 is centred on the 1st. During January (Figure 6 *a–d*), the signal is diluted from week 0 back to week 3, and mainly points to local

terrestrial influence, whereas in June a SW monsoon month (Figure 6 *e–h*), the concentrations at CRI appear to be most sensitive to the fluxes from the Indian Ocean to the south. These conclusions are in agreement with the results obtained for fossil fuel, terrestrial biosphere and oceanic flux tracer simulations.

We have compared observed CO$_2$ mixing ratio at CRI with three transport model simulations (TM3, LMDZ, ACTM) during February 1993–October 2002. Cape Rama is located on the west coast of India and receives marine air during Indian summer monsoon months and terrestrial air during winter months. The trend and mean seasonal cycle of the long-term time series are similar, but most of the observed higher frequency variability is not well captured by the simulations. The seasonal cycle of the simulations has a maximum between February and March, and a minimum in October, whereas observations have their maximum in March and a minimum in November. The root mean square deviation calculated for individual

months indicates that model-observation agreement is better during the SW monsoon months than in the other months. The larger disagreement points to the difficulty in simulating local meteorology (e.g. the land–sea breeze) and local fluxes by the coarse resolution of global models and fluxes at this coastal site. By simulating seasonality in three separate atmospheric tracers to distinguish land, ocean, and fossil-fuel fluxes, we found that land ecosystem and fossil-fuel fluxes have a larger impact than the ocean fluxes on the variability of concentration at CRI, consistent with the strong negative correlation between the CRI $\delta^{13}CO_2$ and CO_2 mixing ratio. Observed growth rate at CRI, averaged during summer and winter months, shows maxima and minima associated with global forcing. Winter growth rates are higher than summer growth rates. Model-simulated CO_2 mixing ratios show weak maxima during strong El Niño events, whereas few of the observed maxima and minima are missing in the models.

Shorter-term influence functions at CRI site have also been studied from the simulations of the adjoint model of LMDZ. The Cape Rama site captures flux signals from diverse regions depending on the time of the year (e.g. the Arabian Sea in June and the northwest part of India in January). It is important to plan a strategic network of atmospheric monitoring sites, developed to ensure that major fluxes from the whole territory are monitored throughout the year. While these data provide useful baseline information on annual to decadal timeframes, to quantitatively link atmospheric concentration/conditions to surface fluxes, and obtain a better understanding of the carbon cycle over the scale of the Indian subcontinent, continuous sampling coupled with high-resolution transport modelling will be required.

1. Boden, T., Marland, G. and Andres, R. J., National CO_2 emissions from fossil-fuel burning, cement manufacture, and gas flaring: 1951–2007. Carbon Dioxide Information Analysis Centre (CDIAC), Oak Ridge National Lab, USA, 8 June 2010, doi 10:3334/CDIAC/00001_v2010.
2. Lal, M. and Singh, R., Carbon sequestration potential of Indian forests. *Environ. Monit. Assess.*, 2000, **60**(3), 315–327.
3. Patra, P. K., Niwa, Y., Schuck, T. J., Brenninkmeijer, C. A. M., Machida, T., Matsueda, H. and Sawa, Y., Carbon balance of South Asia constrained by passenger aircraft CO_2 measurements. *Atmos. Chem. Phys.*, 2011, **11**, 4163–4175.
4. Francey, R. J. *et al.*, The CSIRO (Australia) measurement of greenhouse gasses in the global atmosphere. Report of the Eleventh WMO/IAEA Meeting of Experts on Carbon Dioxide Concentration and Related Tracer Measurement Techniques. WMO GAW Report, 2003, vol. 148, pp. 97–106.
5. Banse, K. and English, D. C., Seasonality of coastal zone colour scanner phytoplankton pigment in the offshore oceans. *J. Geophys. Res.*, 1994, **99**, 7323–7345.
6. Bhattacharya, S. K. *et al.*, Trace gases and CO_2 isotope records from Cabo de Rama, India. *Curr. Sci.*, 2009, **97**, 1336–1344.
7. Francey, R. J., Van der Schoot, M., Krummel, P. B., Trudinger, C. M., Steele, L. P. and Langenfelds, R. L., Differences between trends in atmospheric CO_2 and reported trends in anthropogenic CO_2 emissions. *Tellus*, 2010, **62**, 316–328.
8. Heimann, M. and Körner, S., The global atmospheric tracer model TM3. Model description and user's manual release 3.8a, Max-Planck Institute for Biogeochemistry, Jena, Germany, 2003.
9. Rödenbeck, C., Houweling, S., Gloor, M. and Heimann, M., CO_2 flux history 1982–2001 inferred from atmospheric data using a global inversion of atmospheric tracer transport. *Atmos. Chem. Phys.*, 2003, **3**, 1919–1964.
10. Kalnay, E. *et al.*, The NCEP/NCAR 40-year reanalysis project. *Bull. Am. Meteorol. Soc.*, 1996, **77**, 437–471.
11. Rödenbeck, C., Estimating CO_2 sources and sinks from atmospheric mixing ratio measurements using a global inversion of atmospheric transport. Technical Report 6, Max Planck Institute for Biogeochemistry, Jena, Germany, 2005; http://www.bgcjena.mpg.de/mpg/websiteBiogeochemie/Publikationen/TechnicalReports/tech_report6.pdf.
12. Conway, T., Tans, P. P., Waterman, L. S., Thoning, K. W., Kitzis, D., Masarie, K. and Zhang, N., Evidence for interannual variability of the carbon cycle from the national oceanic and atmospheric administration climate monitoring and diagnostics laboratory global air sampling network. *J. Geophys. Res.*, 1994, **99**, 22831–22855.
13. Hourdin, F. *et al.*, The LMDZ4 general circulation model climate performance and sensitivity to parametrized physics with emphasis on tropical convection. *Climate Dyn.*, 2006, **27**, 787–813.
14. Bousquet, P., Hauglustaine, D. A., Peylin, P., Carouge, C. and Cias, P., Two decades of OH variability as inferred by an inversion of atmospheric transport and chemistry of methyl chloroform. *Atmos. Chem. Phys.*, 2005, **5**, 2635–2656.
15. Chevallier, F. *et al.*, AIRS-based versus surface-based estimation of carbon surface fluxes. *J. Geophys. Res.*, 2009, **114**, D20303.
16. Numaguti, A., Takahashi, M., Nakajima, T. and Sumi, A., Development of CCSR/NIES Atmospheric General Circulation Model, CGER's Supercomputer. *Monogr. Rep.*, 1997, **3**, 1–48.
17. Patra, P. K. *et al.*, Transport mechanisms for synoptic, seasonal and interannual SF_6 variations and 'age' of air in troposphere. *Atmos. Chem. Phys.*, 2009, **9**, 1209–1225.
18. Gurney, K. R. *et al.*, Transcom 3 inversion intercomparison: model mean results for the estimation of seasonal carbon sources and sinks. *Global Biogeochem. Cycles*, 2004, **18**, GB1010.
19. Patra, P. K. *et al.*, Sensitivity of inverse estimation of annual mean CO_2 sources and sinks to ocean – only sites versus all-sites observational networks. *Geophys. Res. Lett.*, 2006, **33**, L05814.
20. Langenfelds, R. L., Francey, R. J., Pak, B. C., Steele, L. P., Lloyd, J., Trudinger, C. M. and Allison, C. E., Interannual growth rate variations of atmospheric CO_2 and its isotope $\delta^{13}C$, H_2, CH_4 and CO between 1992 and 1999 linked to biomass burning. *Global Biogeochem. Cycles*, 2002, **16**(3); 10.1029/2001GB001466
21. Takahashi, T. *et al.*, Global sea-air CO_2 flux based on climatological surface ocean pCO2 and seasonal biological and temperature effects. *Deep Sea Res. II*, 2002, **49**, 1601–1622.
22. Rayner, P. J., Law, R. M., Allison, C. E., Francey, R. J., Trudinger, C. M. and Pickett-Heaps, C., Interannual variability of the global carbon cycle (1992–2005) inferred by inversion of atmospheric CO_2 and $\delta^{13} CO_2$ measurements. *Global Biogeochem. Cycles*, 2008, **22**, GB3008; doi:10.1029/2007GB003068.